

Effect of the Atlantic Multidecadal Variability on the global monsoon

Article

Accepted Version

Monerie, P.-A., Robson, J., Dong, B., Hodson, D. L. R. and Klingaman, N. P. (2019) Effect of the Atlantic Multidecadal Variability on the global monsoon. *Geophysical Research Letters*, 46 (3). pp. 1765-1775. ISSN 0094-8276 doi: <https://doi.org/10.1029/2018GL080903> Available at <http://centaur.reading.ac.uk/82038/>

It is advisable to refer to the publisher's version if you intend to cite from the work. See [Guidance on citing](#).

To link to this article DOI: <http://dx.doi.org/10.1029/2018GL080903>

Publisher: American Geophysical Union

All outputs in CentAUR are protected by Intellectual Property Rights law, including copyright law. Copyright and IPR is retained by the creators or other copyright holders. Terms and conditions for use of this material are defined in the [End User Agreement](#).

www.reading.ac.uk/centaur

CentAUR

Central Archive at the University of Reading

Reading's research outputs online

Effect of the Atlantic Multidecadal Variability on the global monsoon

Paul-Arthur Monerie, Jon Robson, Buwen Dong, Dan Hodson and Nick Klingaman

National Centre for Atmospheric Science, Department of Meteorology, University of Reading

Corresponding email address: p.monerie@reading.ac.uk

Abstract

We assess the effect of the Atlantic Multidecadal Variability (AMV) on the global monsoon using idealized simulations. Warm AMV phases are associated with a significant strengthening of monsoon precipitation over Northern Africa and India, and anomalously weak monsoon precipitation over South America. Changes in monsoon precipitation are mediated by a change in atmospheric dynamics, primarily associated with a shift in the circulation related to both an enhanced interhemispheric thermal contrast and the remote impact of AMV on the Pacific Ocean, through changes in the Walker circulation. In contrast, the thermodynamic changes are less important. Further experiments show that the impact of AMV is largely due to the tropical component of the sea surface temperature anomalies. However, the extratropical Atlantic also plays a role, especially for northern Africa. Finally, we show that the effect of AMV on monsoons is not linearly related to the magnitude of warming.

Key points:

- Changes in atmospheric circulation dominate the AMV effect on monsoons, whilst thermodynamic changes are moderate.
- The tropical North Atlantic largely forces AMV effects, by strengthening inter-hemispheric thermal gradients and the Walker circulation.
- The effects of AMV are not linearly related to the magnitude of warming.

24 1 Introduction

25 The North Atlantic Sea Surface Temperature (NASST) has undergone strong variations on decadal-
26 to-multidecadal scales that are due to internal and external climate variability (Terray, 2012). This
27 variability is called the Atlantic Multidecadal variability (AMV) and has been associated with ocean and
28 atmospheric processes (Delworth et al., 1993; Knight et al., 2005), as well as with volcanic, solar (Otterå
29 et al., 2010) and anthropogenic (Booth et al., 2012) forcing.

30 There is significant evidence to suggest that the AMV has played an important role in recent trends
31 in tropical precipitation (Kamae et al. 2017) and can substantially modulate the global monsoon (GM)
32 system (Trenberth et al., 2000; Wang & Ding, 2008; An et al., 2015; Wang et al., 2017, Wang et al.,
33 2018). For example, AMV influences precipitation over North East Brazil and the Sahel by shifting the
34 location of the Intertropical Convergence Zone (ITCZ) over the tropical Atlantic Ocean (Sutton &
35 Hodson, 2005; Knight et al., 2006). AMV also affects the Indian and the East Asian summer rainfall,
36 through altering the interhemispheric thermal contrast and El-Niño Southern Oscillation (ENSO)
37 variability (Wang et al., 2009; Luo et al., 2017). The positive phase of the AMV can also force an
38 extratropical wavetrain, and can impact the Indian monsoon system (Li et al., 2008). Furthermore, AMV
39 has been linked with changes over the eastern equatorial Pacific Ocean via changes in Walker circulation
40 strength and are also associated with a change in the south Asian summer monsoon (Dong et al., 2006),

41 Wang et al., (2013) have shown an observed relationship between AMV, the Pacific Ocean and the
42 northern hemisphere summer monsoon. However, the complexity of the climate system and the presence
43 of multiple drivers of the global monsoon makes quantifying AMV's impact difficult, and the involved
44 physical processes remain to be elucidated.

45 AMV is also composed of SST anomalies in both the tropical and the extratropical North Atlantic
46 Ocean (Sutton & Hodson, 2007). Generally it is thought that tropical Atlantic anomalies are key to
47 explaining effects of the AMV (Sutton & Hodson, 2007). However, the subpolar North Atlantic SSTs
48 are highly predictable (Robson et al., 2012), and so could be useful to forecast the effect of AMV over
49 land (Robson et al., 2014). Therefore, it is important to understand the relative effects of SST anomalies
50 in each Atlantic sub-domain, and to understand whether the effects are due to changes in atmospheric

51 dynamics (i.e. through changes in circulation) or thermodynamics (i.e. through changes in surface
52 temperature and humidity)?

53 In this study we will use idealized modelling experiments to better understand if, and how, the AMV
54 affects the global monsoon (i.e. the tropical monsoon domains). In particular, we will assess the relative
55 roles of dynamic and thermodynamic changes in generating the anomalies, and the linearity of the
56 response. Section 2 outlines the experiments and precipitation decomposition we employ, section 3
57 describes the main results, and the key conclusions are outlined in section 4.

58

59 2 Model and methods

60 2.1 MetUM-GOML2 and experimental design

61 We use the MetUM-GOML2 model to explore the effect of AMV through idealized experiments.
62 MetUM-GOML2 is the Global Ocean Mixed-Layer coupled configuration of the Met Office Unified
63 Model (MetUM-GOML2; Hirons et al. 2015), comprising the MetUM Global Atmosphere 6.0 (Walters
64 et al., 2017) coupled to the Multi-Column K Profile Parameterisation ocean (MC-KPP, version 1.1) via
65 the Ocean Atmosphere Sea Ice Soil (OASIS) coupler (Valcke, 2013). The atmosphere has a $1.87 \times 1.25^\circ$
66 horizontal resolution ($\sim 135\text{km}$) with 85 vertical levels. The ocean mixed-layer component extends to 1
67 km depth with 100 vertical levels.

68 MC-KPP does not allow ocean advection, and also has prescribed SSTs and sea ice
69 concentrations in regions which are not ice-free throughout the year in the reference climatology (i.e.
70 sea ice is not interactive – see coupling mask in figure S1). In coupled regions a seasonally-varying
71 climatological 3D flux correction is applied to both temperature and salinity to hold the model close to
72 a reference ocean climatology. These fluxes represent the mean ocean advection, and account for biases
73 in atmospheric surface heat and freshwater fluxes. Consequently, MetUM-GOML2 has small SST
74 biases and small model drift relative to coupled models with a fully dynamic ocean (Hirons et al., 2015).
75 We use a 1976-2005 mean ocean temperature and salinity reference climatology derived from the Met
76 Office global statistical ocean reanalysis (MOSORA; Smith & Murphy, 2007). These are used to
77 produce the 3D flux corrections (see Hirons et al, 2015 for details). Outside the coupled region, the
78 atmospheric model is forced by daily SSTs and sea ice from the reference climatology. Anthropogenic
79 greenhouse gas concentrations, aerosol emissions and volcanic activity are imposed and kept constant
80 to their mean value of the period 1976-2005.

81 We follow a slightly modified form of the experimental design from the Decadal Climate
82 Prediction Project (DCPP; Boer et al. 2016). Specifically, an AMV pattern is imposed in the North
83 Atlantic in the model by modifying non-solar heat fluxes (Figure S1 and methodology in the
84 supplementary material). We perform separate experiments to mimic a positive (hereafter called AMV+)

85 and a negative (hereafter called AMV-) phase of the AMV. Unlike in Boer et al. (2016), we multiply
86 the magnitude of the pattern by a factor of two to increase the signal to noise ratio. The targeted pattern
87 is obtained by adding (subtracting) NASST anomalies to (from) the 1976-2005 climatological SSTs and
88 is applied in both coupled and uncoupled regions of the North Atlantic. Note that the additional non-
89 solar heat flux correction is applied only in the targeted region; outside this, SSTs can vary freely through
90 air-sea interaction. Simulations last for 10 years and 4 months and are initialized on 1st September. Note
91 that the simulations last for 10 years when only the tropical Atlantic is warmed. 15 ensemble members
92 are performed for each experiment using different atmospheric initial conditions.

93 We have also performed an experiment where NASST are restored to a climatological state,
94 hereafter called CLM. We also test the role of the tropical and extratropical North Atlantic SST
95 anomalies by warming and cooling the Atlantic Ocean south of 30°N (hereafter called TNA), and north
96 of 30°N (hereafter called XNA), respectively (as defined in DCP-C, see fig. S1). Finally, we also test
97 the linearity of AMV effects by performing additional experiments with a magnitude of one times AMV
98 (hereafter noted 1xAMV) for both negative and positive phases of the AMV (see table S1).

99 2.2 Precipitation metrics

100 Global monsoon domains are defined following Wang et al., (2011), selecting land grid points
101 where the annual precipitation range (i.e. the difference between May to September (MJJAS) and
102 November to March (NDJFM)) exceeds 2.5 mm.day^{-1}) using the CLM simulation. Monsoon domains
103 are NAM (North AMerica), NAF (North AFrica), SAS (South ASia) and EAS (East ASia) in the
104 Northern Hemisphere and SAM (South AMerica), SAF (Southern AFrica) and AUS (AUStralia) in the
105 Southern Hemisphere (Figure 1a). We then compute the area-averaged precipitation of each monsoon
106 domain (MI; Monsoon Index). Note that NAF and SAS domains are smaller than in observations due to
107 large dry biases in MetUM-GOML2 over West Africa and India (Figure S2), as also seen in other
108 MetUM configurations (Walters et al., 2017). However, using domains defined from GPCC, or based
109 on an alternative method (i.e. using a relative threshold), does not alter our conclusions (FigS3 and
110 information in the supplementary material).

111 Monsoon area (MA) is the area of each monsoon domain, as a percentage of the Earth's total
 112 surface. Monsoon total precipitation (MP) is the area weighted sum of precipitation in each monsoon
 113 domain (Zhou et al., 2008; Hsu et al., 2011; Kitoh et al., 2013). These two metrics complement MI since
 114 they quantify the amount of precipitation resulting from changes in both domain size and monsoon
 115 intensities. Unlike MI, MA and MP are computed using a dynamic monsoon domain size (i.e. computed
 116 for each simulation).

117 We decompose precipitation change (ΔP) into its dynamical (ΔP_{dyn}), thermodynamical (ΔP_{therm})
 118 and its non-linear cross components (ΔP_{cross}) following Chadwick et al. (2016). This method relies on
 119 the fact that tropical precipitation is dominated by convection (Chadwick et al., 2016; Rowell &
 120 Chadwick, 2018). If precipitation, P , is represented as $P = M^*q$, where M^* is a proxy for convective
 121 mass flux from the boundary layer to the free troposphere (Held & Soden, 2006; Kent et al., 2015) (M^*
 122 = P/q), and q is near surface specific humidity, then, the change in precipitation, ΔP , can be reformulated
 123 as

$$124 \quad \Delta P = M^*\Delta q + q\Delta M^* + \Delta q\Delta M^* = \Delta P_{\text{therm}} + \Delta P_{\text{dyn}} + \Delta P_{\text{cross}}$$

125 Where ΔP_{therm} represents the contribution from specific humidity changes (q), ΔP_{dyn} represents
 126 the contribution from circulation changes (M^*), and ΔP_{cross} represents the contribution from changes in
 127 both specific humidity and circulation. Terms are first calculated using the monthly mean data and for
 128 each grid point and then averaged over each season and monsoon domain.

129 Further decomposition of ΔP_{dyn} allows us to document changes due to shifts in the pattern of
 130 circulation (ΔP_{shift}) or the mean tropical circulation strength ($\Delta P_{\text{strength}}$), as

$$131 \quad \Delta P_{\text{strength}} = q\Delta M^*_{\text{strength}} \text{ and } \Delta P_{\text{shift}} = q\Delta M^*_{\text{shift}}$$

132 where $\Delta M^*_{\text{strength}} = -\alpha M^*$ with $\alpha = \text{tropical mean } \Delta M^* / \text{tropical mean } M^*$ represents the change
 133 in the strength of the mean tropical circulation. Note that although ΔM^* is a scalar, $\Delta P_{\text{strength}}$ is provided
 134 for each grid point by multiplying by the reference moisture field.

135 $\Delta M^*_{\text{shift}}$ is calculated as the residual of ΔM^* from $\Delta M^*_{\text{strength}}$

136 3. Results

137 3.1 Change in global monsoon precipitation

138 Figure 1a shows the observed relationship between AMV and precipitation, and confirms that
139 AMV is associated with significant changes in observed tropical precipitations (Figure S9; (Trenberth
140 & Shea, 2006; Ting et al., 2011). Figure 1b shows the simulated effect of AMV on precipitation over
141 the summer hemisphere by taking the difference between the AMV+ and AMV- experiments. Positive
142 AMV is associated with a northward shift of the ITCZ over the Atlantic Ocean, leading to increased
143 precipitation in the Northern Hemisphere and decreased precipitation in the Southern Hemisphere
144 (Figure 1b). There are also significant changes in precipitation over the West Pacific warm pool, the
145 northern Indian Ocean and North East India. In contrast, precipitation decreases over northern Australia
146 and Eastern Brazil. As a consequence, precipitation changes are significant over SAM, AUS, NAF and
147 SAS (Figure 1c). However, precipitation changes are not significant for NAM, SAF and EAS, and for
148 GM due to opposing responses between the Northern and the Southern hemispheres. Note the
149 comparison of simulated and observed precipitation patterns highlights differences over the Amazon
150 Basin and over Southern Africa, which we will discuss in section 4.

151 There are also significant changes in MA and MP (Figure 1d). Monsoon extent is closely linked
152 to changes in total monsoon precipitation in all monsoon domains. In positive AMV, SAM and AUS
153 monsoon domains are considerably smaller, while other monsoon domains become wider, especially
154 SAS, NAF and EAS (Figure 1d and Figure S4).

155 3.2 Decomposition of AMV monsoon impacts

156 Figure 2 shows the decomposition of monsoon rainfall into dynamic and thermodynamic
157 components, and their nonlinear combination. In most domains ΔP_{dyn} is larger than ΔP_{therm} , indicating
158 that the atmospheric circulation change dominates the impact of AMV on the global monsoons (Figure
159 2a and Figure 2b). Moreover, the spatial distribution of ΔP_{dyn} is extremely similar to ΔP (Figure S5).
160 ΔP_{therm} exhibits a clear inter-hemispheric pattern, consistent with the surface temperature increase, which

161 is mainly confined to the Northern Hemisphere (Figure 3a and Figure 3b). Finally, the nonlinear term
162 tends to increase precipitation in all monsoon domains (Figure 2c). Therefore, the change in precipitation
163 is due to a combination of changes in the three terms. The weak changes in SAM, NAM and EAS
164 precipitation are the result of opposing effects from ΔP_{dyn} , ΔP_{cross} and ΔP_{therm} .

165 To explore ΔP_{dyn} further, we decompose the circulation response into changes in the mean
166 tropical circulation strength ($\Delta P_{\text{strength}}$) or shifts in atmospheric circulation patterns (ΔP_{shift}). $\Delta P_{\text{strength}}$ is
167 almost negligible, but explains a small increase in precipitation as a response to AMV (Figure 2e). In
168 contrast, ΔP_{shift} is generally larger. Therefore, ΔP_{dyn} (and, hence, ΔP) is due to a shift in atmospheric
169 circulation, rather than to a modulation of its mean strength (Figure 2d). Moreover, ΔP_{shift} clearly
170 dominates the pattern of ΔP_{dyn} and, by extension, of ΔP (Figure S5). The importance of a shift in
171 circulation, on simultaneous changes in both q and M^* , also helps to explain why ΔP_{cross} plays a
172 significant role.

173 3.3 AMV's impact on surface temperature and atmospheric circulation

174 To better understand how AMV affects the global monsoon regions, we analyze changes in
175 surface temperature, 200 hPa velocity potential and low-level wind. In NDJFM and MJJAS the warming
176 of the North Atlantic (Figure 3a and Figure 3b) causes the ITCZ to shift northward, hence increasing
177 NAF precipitation and decreasing precipitation over South America (Knight et al., 2006) through
178 strengthening the Atlantic trade winds (Figure 3e and Figure 3f). Surface temperature also increases
179 over the Eurasian continent in NDJFM and MJJAS, but not over the Indian Ocean (Figure 3a and Figure
180 3b). Thus, the enhanced South Asian Monsoon is consistent with an increased land-ocean thermal
181 contrast driving a stronger monsoon circulation, as seen in the low-level wind anomalies (Figure 3f) in
182 line with the observations (Wang et al., 2013).

183 Over Australia and the Maritime Continent, a decrease in winter precipitation is associated with
184 low-level wind divergence (Figure 3e) and increased subsidence over the western Pacific Ocean (Figure
185 3c). A cooling of the eastern Pacific Ocean and a warming of the western and North Pacific Ocean is
186 consistent with the positive AMV forcing a shift to a negative phase of the Interdecadal Pacific

187 Oscillation (IPO) (Zhang et al., 1997; Ruprich-Robert et al., 2017; Figure S6) (Figure 3ab). Here, the
188 cooling in the eastern Pacific Ocean is the result of changes in the Walker circulation forced by
189 anomalously strong ascent over the Atlantic Ocean and India, which are both a result of warming
190 Atlantic SSTs (Figure 3 cd). Changes in tropical eastern Pacific temperature in turn impact summer
191 Indian precipitation, as there is a strong relationship between the Indian summer monsoon and ENSO
192 (Yun & Timmermann, 2018).

193 3.4 Tropical, extratropical warming and linearity of the effects

194 We now explore the effects that are driven by tropical or extratropical AMV SSTs. Warming the
195 tropical North Atlantic (TNA) leads to negative anomalies in SAM, and positive anomalies in NAF and
196 SAS precipitation (Figure 4a). The impact of warm TNA SSTs on North East Brazilian and Sahel
197 precipitation is related to anomalously strong cyclonic circulation over the tropical Atlantic and the
198 Caribbean Sea (Figure 4c-d), which leads to divergence over South America and convergence over the
199 equatorial eastern Atlantic Ocean and Sahel. Increased SAS precipitation is associated with a
200 strengthening of the southwesterly Indian monsoon flows, in association with an increase in the inter-
201 hemispheric thermal gradient and a strengthening of the trade winds (Figure 4d and Figure S7).

202 A warmer extratropical North Atlantic (XNA) significantly affects the North African Monsoon by
203 shifting the ITCZ northward over western Africa and the Sahel (Figure 4b, consistent with Dunstone et
204 al., 2011). Therefore, both TNA and XNA SST anomalies are important to explain the impacts of AMV
205 on NAF and NAM domains. However, unlike TNA, XNA does not significantly affect the Pacific Ocean,
206 or the Indian Ocean via Walker circulation changes (Figure S6), and, hence, does not affect SAS
207 precipitation. Changes in tropical low-level circulation are also mostly explained by the tropical Atlantic
208 Ocean SSTs, explaining the lack of changes over other monsoon domains in the XNA experiment
209 (Figure 4e-f). Differences in SAS precipitation changes are also associated with differences in the
210 strengthening of the Walker circulation, largely stronger in TNA than in XNA (Figure S8).

211 We note that the effects of AMV are also non-linear to the magnitude of the Atlantic warming. For
212 example, although the patterns of simulated anomalies are similar (i.e. increase in NAF and SAS and

213 decrease in SAM precipitation) the impacts on monsoon precipitation in the AMV experiment are only
214 1.44 times stronger than in the 1xAMV simulations (Figure 4g; table S2). Furthermore, the sum of TNA
215 and XNA experiments again yields similar anomalies to that of the full AMV experiment, but with a
216 stronger magnitude. Therefore, this non-linearity suggests that there are interference between the
217 response to both TNA and XNA, as proposed in Qasmi et al. (2017).

218

219 4. Conclusions and discussion

220 We assessed the effect of the Atlantic Multidecadal Variability (AMV) on global monsoon
221 subdomains in a coupled Atmosphere-Ocean Mixed Layer model (MetUM-GOML2) using idealized
222 SST nudging experiments. Experiments are performed to test the effect of the whole AMV as well as
223 the tropical and extratropical parts of AMV. The key results are as follows

- 224 - The AMV affects the global monsoon significantly in terms of mean precipitation, total
225 precipitation, and monsoon area. The monsoon strengthens over Northern Africa, and South
226 Asia, and weakens over South America and Australia. However, the effect on the globally
227 integrated monsoon precipitation is not significantly different to zero.
- 228 - The effect of AMV on regional monsoons is mostly due to the dynamic response, rather than
229 the thermodynamic response. Furthermore, the dynamical response is due to a shift in the
230 atmospheric circulation, rather than changes in the strength of the mean tropical circulation. For
231 example, a northward shift of the ITCZ over the Atlantic Ocean and a shift to a negative phase
232 of the IPO play a crucial role. This shift in the atmospheric circulation accounts for the important
233 contributions of the nonlinear term.
- 234 - The thermodynamic term plays a lesser role but has a significant effect on hemispheric contrast,
235 enhancing (reducing) monsoon precipitation in the northern (southern) hemisphere due to the
236 interhemispheric temperature contrast caused by AMV.
- 237 - SST anomalies in the tropical North Atlantic (TNA) explain most of the changes in global
238 monsoons related to the AMV (i.e. decrease in SAM precipitation, increase in NAF and SAS

239 precipitation). However, SST anomalies in the extratropical Atlantic also have significant
240 effects, particularly over northern Africa. Therefore, both TNA and XNA must be considered
241 to explain the impact of AMV on the global monsoon variability.

242 - Changes in the global monsoon are sensitive to the magnitude of the imposed AMV forcing.
243 Experiments with one or two times AMV simulate very similar patterns of precipitation
244 anomalies, but the magnitude of the response is less than two times stronger in the latter than in
245 the former. Similarly, the sum of TNA and XNA experiments yield to an overall stronger
246 precipitation anomaly than the full AMV anomalies.

247 These results further highlight the important societal effects of AMV, via its significant modulation of
248 tropical precipitation (as seen in Ting et al., 2009b). For instance, a strong and linear relationship is
249 obtained between changes in Monsoon Area and changes in Monsoon Precipitation indicating that in
250 some regions, like SAS, a larger population is impacted by the monsoon during positive phases of AMV.
251 Results also clarify, for the first time, that the atmospheric circulation response is crucial to generate the
252 impact of AMV on the global monsoon subdomains. Additionally, results have highlighted the complex
253 nonlinear nature of AMV impacts in terms of the magnitude of NASST warming and the location of the
254 warming (e.g. over the tropical or the extratropical North Atlantic Ocean).

255 Although we have shown a significant impact of AMV on the monsoons, there are several
256 caveats. The model is also not able to reproduce the observed link between AMV and SAM or SAF
257 precipitation (Figure S9). For example, MetUM-GOML2 simulates a large decrease in SAM
258 precipitation (Fig. 1b), while observations shows a positive correlation between NASST and winter
259 Amazonian precipitation (Villamayor et al., 2017) (Figure S9). These differences may be related to mean
260 state biases (see Fig. S2). However, comparisons between observations and idealized simulations is not
261 trivial, due to the lack of changes in external forcing or internal variability. Additionally, like most
262 climate models (Schumacher & Houze, 2003), MetUM-GOML2 overestimates the importance of
263 convective precipitation in the total precipitation (not shown), and uncertainties could remain in
264 decomposing precipitation over the subtropical part of the monsoon domains. Finally, the analysis
265 presented here relies on only one climate model, which does not have a fully dynamic ocean model and,

266 hence, may not represent all the relevant ocean feedbacks. Future work should focus on multi model
267 analysis, as proposed in DCCP-C (Boer et al, 2016).

268

269

270 Captions:

271 Figure 1: (a) Observed precipitation ($\text{mm}\cdot\text{day}^{-1}$; GPCC; (Schneider et al., 2014)) regressed onto the
272 AMV index (ERSST; (Huang et al., 2015)) (See the method in the supplementary material). (b) Change
273 in precipitation ($\text{mm}\cdot\text{day}^{-1}$) related to AMV (AMV+ minus AMV-). Monsoon domains are drawn in red
274 (see section 2.2 for details). Precipitation anomalies are shown for MJJAS (NDJFM) for the Northern
275 (Southern) Hemisphere. Stippling indicates that anomalies are significantly different to zero according
276 to a Student's t-test at the 95% confidence level. (c) Changes in monsoon index (MI; $\text{mm}\cdot\text{day}^{-1}$) for
277 AMV+ minus AMV-. A blue bar indicates significant changes according to a Student's t-test at the 95%
278 confidence level. Orange vertical lines show two standard errors. (d) Change in monsoon area (MA; %
279 of the Earth total surface) versus the change in monsoon precipitation (MP; total area weighed
280 precipitation, in $10^9 \text{ m}^3\cdot\text{day}^{-1}$). Vertical and horizontal colored lines indicate two standard errors for both
281 MP and MA. The black line is the MA—MP linear regression (excluding GM). For (c) monsoon
282 domains are not fixed and computed separately from each member and experiment.

283 Figure 2: Decomposition of precipitation anomalies ($\text{mm}\cdot\text{day}^{-1}$) into those due to (a) dynamic (ΔP_{dyn}) (b)
284 thermodynamic (ΔP_{therm}) and (c) cross-term (ΔP_{cross}) terms, as defined in Chadwick et al. (2016). The
285 dynamic part is decomposed into its (e) shift (ΔP_{shift} , i.e. due to a change in the pattern of the circulation)
286 and (f) weak ($\Delta P_{\text{strength}}$, i.e. related to the strength of the mean tropical circulation) components. Orange
287 vertical lines represent two standard errors. A blue bar is added when anomalies are stronger than two
288 standard errors.

289 Figure 3: Effect of AMV on (top panels) surface temperature ($^{\circ}\text{C}$), (middle) 250 hPa velocity potential
290 (in $10^4 \text{ m}^2 \text{ s}^{-1}$) and divergent wind ($\text{m}\cdot\text{s}^{-1}$) and (bottom) sea level pressure (Pa) and 850 hPa wind ($\text{m}\cdot\text{s}^{-1}$),
291 in (left) NDJFM and (right) MJJAS. Stippling (shading) for surface temperature (velocity potential)
292 indicates that changes are significantly different to zero according to a Student's t-test at the 95%
293 confidence level. For the 850 hPa wind, arrows are drawn only if their meridional or zonal components
294 are significantly different to zero, according to a Student's t-test at the 95% confidence level.

295 Figure 4: Top panels: same as in figure 1b but for (a) the tropical Atlantic Ocean warming (TNA+ minus
296 TNA-) and (b) due to the extratropical Atlantic Ocean warming (XNA+ minus XNA-). Middle panels:
297 same as in figure 3a and figure 3b, but for TNA and XNA. Bottom panels: effect of 2xAMV on MI in
298 function of the effect of (left) 1xAMV on MI (right) the TNA+XNA sum on MI. Vertical and horizontal
299 black lines indicate the spread in MI, and the black line is the linear regression, as computed from the
300 sub-domain monsoons only (e.g. excluding GM). Significance in panels a-f are calculated using a
301 Student's t-test at the 95% confidence level.

302

303 **Acknowledgements** The authors gratefully acknowledge support from the UK–China Research and
304 Innovation Partnership Fund through the Met Office Climate Science for Service Partnership (CSSP)
305 China as part of the Newton Fund. BD, DH and JR were supported by the Natural Environment Research
306 Council (NERC) via the National Centre for Atmospheric Science (NCAS), and JR was additionally
307 funded by the NERC ACSIS program. NK was supported by a NERC Independent Research Fellowship
308 (NE/L010976/1). Assembly of MetUM-GOML and development of MC-KPP was supported by the
309 National Centre for Atmospheric Science and led by Dr. Nicholas Klingaman. The authors thank the
310 two anonymous reviewers for their constructive comments and suggestions. The data set used for this
311 study is freely available on <http://doi.org/10.5281/zenodo.2386272>. Additional data will be available
312 through the EU PRIMAVERA project and will be published in due course at BADC via ESGF.

313

314

315

316 Plain language summary

317 Global monsoon precipitation variability has substantial effects on about two-thirds of the world's
318 population. Therefore, understanding the factors that drive tropical precipitation is societally important.
319 Here we focus on the effect of North Atlantic Sea Surface Temperature (NASST) variability on global
320 monsoon. To do so we use a set of climate model experiments, in which we add a surface temperature
321 anomaly over the North Atlantic Ocean. The novelty of the analysis relies on the decomposition of
322 precipitation changes to understand better their origins. We find that NASST changes have strong
323 impacts on Sahel and Indian summer precipitation and monsoon domain sizes, through shifting
324 northward the atmospheric patterns of moisture convergence. Changes involve increases in the large-
325 scale warming of the northern Hemisphere and forcing of the eastern equatorial Pacific Ocean
326 temperature. We highlight the tropical Atlantic basin as critical to explain the effects of NASST
327 variability over the global monsoon. We found that changes in monsoon precipitation are sensitive to
328 the magnitude of the NASST warming.

329

330

331

332 References

- 333 An, Z., Wu, G., Li, J., Sun, Y., Liu, Y., Zhou, W., et al. (2015). Global Monsoon Dynamics and
334 Climate Change. *Annual Review of Earth and Planetary Sciences*, 43(1), 29–77. JOUR.
335 <https://doi.org/10.1146/annurev-earth-060313-054623>
- 336 Ba, J., Keenlyside, N. S., Latif, M., Park, W., Ding, H., Lohmann, K., et al. (2014). A multi-model
337 comparison of Atlantic multidecadal variability. *Climate Dynamics*, 43(9), 2333–2348. article.
338 <https://doi.org/10.1007/s00382-014-2056-1>
- 339 Bellomo, K., Murphy, L. N., Cane, M. A., Clement, A. C., & Polvani, L. M. (2017). Historical
340 forcings as main drivers of the Atlantic multidecadal variability in the CESM large ensemble.
341 *Climate Dynamics*. article. <https://doi.org/10.1007/s00382-017-3834-3>
- 342 Boer, G. J., Smith, D. M., Cassou, C., Doblas-Reyes, F., Danabasoglu, G., Kirtman, B., et al. (2016).
343 The Decadal Climate Prediction Project (DCPP) contribution to CMIP6. *Geoscientific Model*
344 *Development*, 9(10), 3751–3777. article. <https://doi.org/10.5194/gmd-9-3751-2016>
- 345 Booth, B. B. B., Dunstone, N. J., Halloran, P. R., Andrews, T., & Bellouin, N. (2012). Aerosols
346 implicated as a prime driver of twentieth-century North Atlantic climate variability. *Nature*,
347 484(7393), 228–232. <https://doi.org/10.1038/nature10946>
- 348 Chadwick, R., Good, P., & Willett, K. (2016). A Simple Moisture Advection Model of Specific
349 Humidity Change over Land in Response to SST Warming. *Journal of Climate*, 29(21), 7613–
350 7632. JOUR. <https://doi.org/10.1175/JCLI-D-16-0241.1>
- 351 Clement, A., Bellomo, K., Murphy, L. N., Cane, M. A., Mauritsen, T., Rädel, G., & Stevens, B.
352 (2015). The Atlantic Multidecadal Oscillation without a role for ocean circulation. *Science*,
353 350(6258), 320–324. article. <https://doi.org/10.1126/science.aab3980>
- 354 Delworth, T., & Mann, M. (2000). Observed and simulated multidecadal variability in the Northern
355 Hemisphere. *Climate Dynamics*, 16(9), 661–676. article. <https://doi.org/10.1007/s003820000075>
- 356 Delworth, T. L., Manabe, S., & Stouffer, R. J. (1993). Interdecadal Variations of the Thermohaline
357 Circulation in a Coupled Ocean-Atmosphere Model. *Journal of Climate*, 6(11), 1993–2011.
358 JOUR. [https://doi.org/10.1175/1520-0442\(1993\)006<1993:IVOTTC>2.0.CO;2](https://doi.org/10.1175/1520-0442(1993)006<1993:IVOTTC>2.0.CO;2)
- 359 Dong, B., Sutton, R. T., & Scaife, A. A. (2006). Multidecadal modulation of El Niño–Southern
360 Oscillation (ENSO) variance by Atlantic Ocean sea surface temperatures. *Geophysical Research*
361 *Letters*, 33(8). JOUR. <https://doi.org/10.1029/2006GL025766>
- 362 Dunstone, N. J., Smith, D. M., & Eade, R. (2011). Multi-year predictability of the tropical Atlantic
363 atmosphere driven by the high latitude North Atlantic Ocean. *Geophysical Research Letters*,
364 38(14), n/a–n/a. article. <https://doi.org/10.1029/2011GL047949>
- 365 Held, I. M., & Soden, B. J. (2006). Robust Responses of the Hydrological Cycle to Global Warming.
366 *Journal of Climate*, 19(21), 5686–5699. JOUR. <https://doi.org/10.1175/JCLI3990.1>
- 367 Hirons, L. C., Klingaman, N. P., & Woolnough, S. J. (2015). MetUM-GOML: a near-globally coupled
368 atmosphere–ocean-mixed-layer model. *Geoscientific Model Development*, 8, 363–379. JOUR.
- 369 Hsu, P., Li, T., & Wang, B. (2011). Trends in global monsoon area and precipitation over the past 30
370 years. *Geophysical Research Letters*, 38(8). JOUR. <https://doi.org/doi:10.1029/2011GL046893>
- 371 Huang, B., Banzon, V. F., Freeman, E., Lawrimore, J., Liu, W., Peterson, T. C., et al. (2015).
372 Extended Reconstructed Sea Surface Temperature Version 4 (ERSST.v4). Part I: Upgrades and

373 Intercomparisons. *Journal of Climate*, 28(3), 911–930. article. [https://doi.org/10.1175/JCLI-D-](https://doi.org/10.1175/JCLI-D-14-00006.1)
374 14-00006.1

375 Kamae, Y., Li, X., Xie, S.-P., & Ueda, H. (2017). Atlantic effects on recent decadal trends in global
376 monsoon. *Climate Dynamics*. article. <https://doi.org/10.1007/s00382-017-3522-3>

377 Kent, C., Chadwick, R., & Rowell, D. P. (2015). Understanding Uncertainties in Future Projections of
378 Seasonal Tropical Precipitation. *Journal of Climate*, 28(11), 4390–4413. JOUR.
379 <https://doi.org/10.1175/JCLI-D-14-00613.1>

380 Kitoh, A., Endo, H., Krishna Kumar, K., Cavalcanti, I. F. A., Goswami, P., & Zhou, T. (2013).
381 Monsoons in a changing world: A regional perspective in a global context. *Journal of*
382 *Geophysical Research: Atmospheres*, 118(8), 3053–3065. article.
383 <https://doi.org/10.1002/jgrd.50258>

384 Knight, J. R., Allan, R. J., Folland, C. K., Vellinga, M., & Mann, M. E. (2005). A signature of
385 persistent natural thermohaline circulation cycles in observed climate. *Geophysical Research*
386 *Letters*, 32(20), n/a–n/a. article. <https://doi.org/10.1029/2005GL024233>

387 Knight, J. R., Folland, C. K., & Scaife, A. A. (2006). Climate impacts of the Atlantic Multidecadal
388 Oscillation. *Geophysical Research Letters*, 33(17), L17706.
389 <https://doi.org/10.1029/2006GL026242>

390 Kucharski, F., Kang, I.-S., Farneti, R., & Feudale, L. (2011). Tropical Pacific response to 20th century
391 Atlantic warming. *Geophysical Research Letters*, 38(3). JOUR.
392 <https://doi.org/10.1029/2010GL046248>

393 Li, S., Perlwitz, J., Quan, X., & Hoerling, M. P. (2008). Modelling the influence of North Atlantic
394 multidecadal warmth on the Indian summer rainfall. *Geophysical Research Letters*, 35(5). article.
395 <https://doi.org/10.1029/2007GL032901>

396 Luo, F., Li, S., Gao, Y., Keenlyside, N., Svendsen, L., & Furevik, T. (2017). The connection between
397 the Atlantic multidecadal oscillation and the Indian summer monsoon in CMIP5 models. *Climate*
398 *Dynamics*. JOUR. <https://doi.org/10.1007/s00382-017-4062-6>

399 Martin, E. R., & Thorncroft, C. D. (2014). The impact of the AMO on the West African monsoon
400 annual cycle. *Quarterly Journal of the Royal Meteorological Society*, 140(678), 31–46.
401 <https://doi.org/10.1002/qj.2107>

402 McGregor, S., Timmermann, A., Stuecker, M. F., England, M. H., Merrifield, M., Jin, F.-F., &
403 Chikamoto, Y. (2014). Recent Walker circulation strengthening and Pacific cooling amplified by
404 Atlantic warming. *Nature Climate Change*, 4, 888. JOUR. Retrieved from
405 <http://dx.doi.org/10.1038/nclimate2330>

406 Msadek, R., Delworth, T. L., Rosati, A., Anderson, W., Vecchi, G., Chang, Y.-S., et al. (2014).
407 Predicting a Decadal Shift in North Atlantic Climate Variability Using the GFDL Forecast
408 System. *Journal of Climate*, 27(17), 6472–6496. <https://doi.org/10.1175/JCLI-D-13-00476.1>

409 Otterå, O. H., Bentsen, M., Drange, H., & Suo, L. (2010). External forcing as a metronome for
410 Atlantic multidecadal variability. *Nature Geoscience*, 3, 688. JOUR. Retrieved from
411 <http://dx.doi.org/10.1038/ngeo955>

412 Robson, J., Sutton, R., & Smith, D. (2014). Decadal predictions of the cooling and freshening of the
413 North Atlantic in the 1960s and the role of ocean circulation. *Climate Dynamics*, 42(9–10),
414 2353–2365. <https://doi.org/10.1007/s00382-014-2115-7>

415 Robson, J. I., Sutton, R. T., & Smith, D. M. (2012). Initialized decadal predictions of the rapid
416 warming of the North Atlantic Ocean in the mid 1990s. *Geophysical Research Letters*, 39(19),

417 n/a-n/a. <https://doi.org/10.1029/2012GL053370>

418 Rowell, D. P., & Chadwick, R. (2018). Causes of the Uncertainty in Projections of Tropical Terrestrial
419 Rainfall Change: East Africa. *Journal of Climate*. JOUR. <https://doi.org/10.1175/JCLI-D-17->
420 0830.1

421 Ruprich-Robert, Y., Msadek, R., Castruccio, F., Yeager, S., Delworth, T., & Danabasoglu, G. (2017).
422 Assessing the Climate Impacts of the Observed Atlantic Multidecadal Variability Using the
423 GFDL CM2.1 and NCAR CESM1 Global Coupled Models. *Journal of Climate*, 30(8), 2785–
424 2810. JOUR. <https://doi.org/10.1175/JCLI-D-16-0127.1>

425 Schneider, U., Becker, A., Finger, P., Meyer-Christoffer, A., Ziese, M., & Rudolf, B. (2014). GPCP's
426 new land surface precipitation climatology based on quality-controlled in situ data and its role in
427 quantifying the global water cycle. *Theoretical and Applied Climatology*, 115(1–2), 15–40.
428 <https://doi.org/10.1007/s00704-013-0860-x>

429 Schumacher, C., & Houze, R. A. (2003). Stratiform Rain in the Tropics as Seen by the TRMM
430 Precipitation Radar. *Journal of Climate*, 16(11), 1739–1756. JOUR.
431 [https://doi.org/10.1175/1520-0442\(2003\)016<1739:SRITTA>2.0.CO;2](https://doi.org/10.1175/1520-0442(2003)016<1739:SRITTA>2.0.CO;2)

432 Smith, D. M., & Murphy, J. M. (2007). An objective ocean temperature and salinity analysis using
433 covariances from a global climate model. *Journal of Geophysical Research*, 112(C2), C02022.
434 <https://doi.org/10.1029/2005JC003172>

435 Sutton, R., & Hodson, D. (2007). Climate Response to Basin-Scale Warming and Cooling of the North
436 Atlantic Ocean. *Journal of Climate*, 20(5), 891–907. JOUR. <https://doi.org/10.1175/JCLI4038.1>

437 Sutton, R. T., & Hodson, D. L. R. (2005). Atlantic Ocean Forcing of North American and European
438 Summer Climate. *Science*, 309(5731), 115–118. article. <https://doi.org/10.1126/science.1109496>

439 Terray, L. (2012). Evidence for multiple drivers of North Atlantic multi-decadal climate variability.
440 *Geophysical Research Letters*, 39(19). article. <https://doi.org/10.1029/2012GL053046>

441 Ting, M., Kushnir, Y., Seager, R., & Li, C. (2009). Forced and Internal Twentieth-Century SST
442 Trends in the North Atlantic. *Journal of Climate*, 22(6), 1469–1481. article.
443 <https://doi.org/10.1175/2008JCLI2561.1>

444 Ting, M., Kushnir, Y., Seager, R., & Li, C. (2011). Robust features of Atlantic multi-decadal
445 variability and its climate impacts. *Geophysical Research Letters*, 38(17). JOUR.
446 <https://doi.org/10.1029/2011GL048712>

447 Trenberth, K. E., & Shea, D. J. (2006). Atlantic hurricanes and natural variability in 2005.
448 *Geophysical Research Letters*, 33(12). article. <https://doi.org/10.1029/2006GL026894>

449 Trenberth, K. E., Stepaniak, D. P., & Caron, J. M. (2000). The Global Monsoon as Seen through the
450 Divergent Atmospheric Circulation. *Journal of Climate*, 13(22), 3969–3993. JOUR.
451 [https://doi.org/10.1175/1520-0442\(2000\)013<3969:TGMASST>2.0.CO;2](https://doi.org/10.1175/1520-0442(2000)013<3969:TGMASST>2.0.CO;2)

452 Valcke, S. (2013). The OASIS3 coupler: a European climate modelling community software.
453 *Geoscientific Model Development*, 6(2), 373–388. <https://doi.org/10.5194/gmd-6-373-2013>

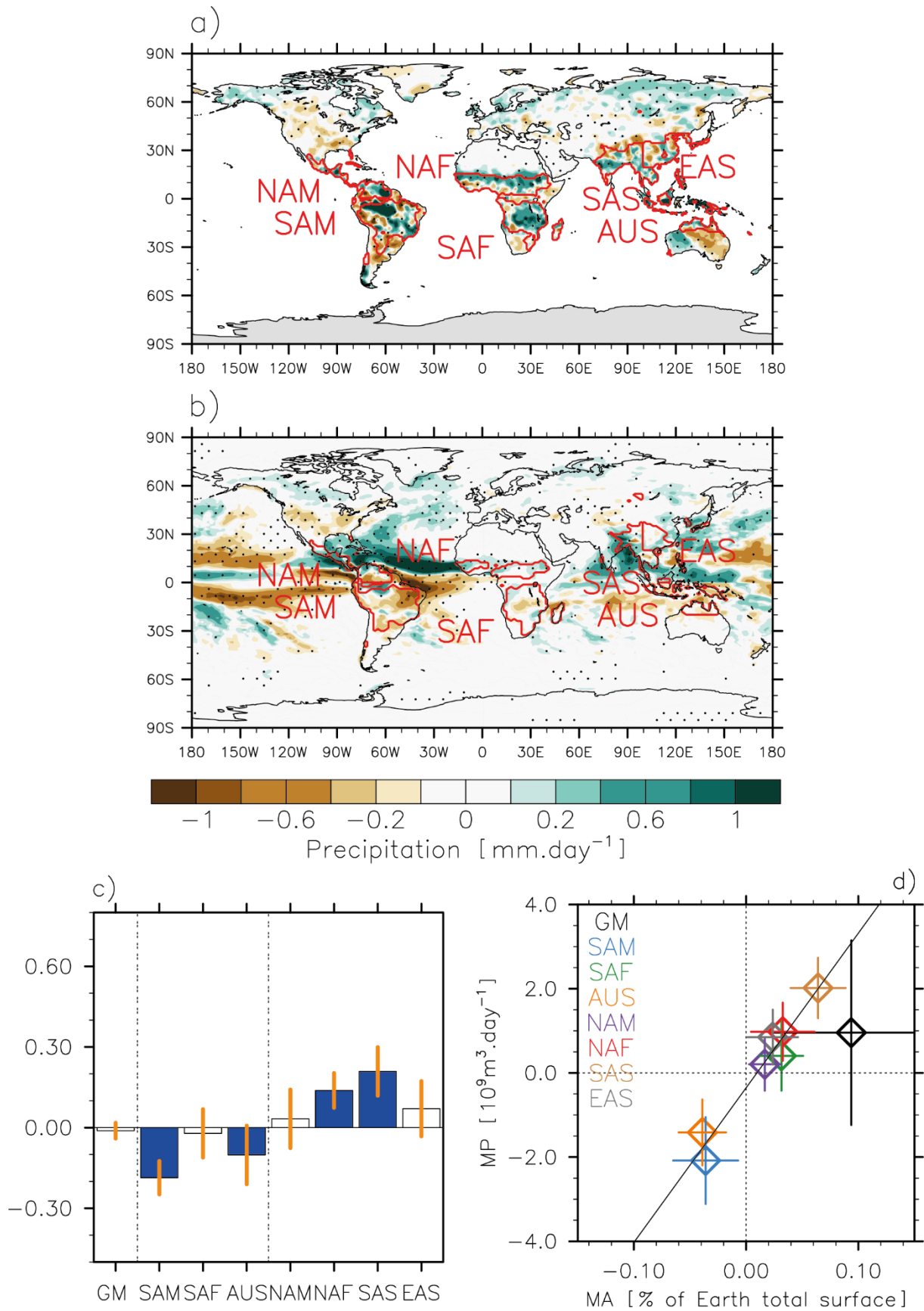
454 Villamayor, J., Ambrizzi, T., & Mohino, E. (2017). Influence of decadal sea surface temperature
455 variability on northern Brazil rainfall in CMIP5 simulations. *Climate Dynamics*. JOUR.
456 <https://doi.org/10.1007/s00382-017-3941-1>

457 Walters, D., Boutle, I., Brooks, M., Melvin, T., Stratton, R., Vosper, S., et al. (2017). The Met Office
458 Unified Model Global Atmosphere 6.0/6.1 and JULES Global Land 6.0/6.1 configurations.
459 *Geoscientific Model Development*, 10(4), 1487–1520. article. <https://doi.org/10.5194/gmd-10->

- 460 1487-2017
- 461 Wang, B., & Ding, Q. (2008). Global monsoon: Dominant mode of annual variation in the tropics.
 462 *Dynamics of Atmospheres and Oceans*, 44(3), 165–183. JOUR.
 463 <https://doi.org/https://doi.org/10.1016/j.dynatmoce.2007.05.002>
- 464 Wang, B., Kim, H.-J., Kikuchi, K., & Kitoh, A. (2011). Diagnostic metrics for evaluation of annual
 465 and diurnal cycles. *Climate Dynamics*, 37(5), 941–955. JOUR. [https://doi.org/10.1007/s00382-](https://doi.org/10.1007/s00382-010-0877-0)
 466 010-0877-0
- 467 Wang, B., Liu, J., Kim, H.-J., Webster, P. J., Yim, S.-Y., & Xiang, B. (2013). Northern Hemisphere
 468 summer monsoon intensified by mega-El Niño/southern oscillation and Atlantic multidecadal
 469 oscillation. *Proceedings of the National Academy of Sciences*, 110(14), 5347 LP-5352. JOUR.
 470 Retrieved from <http://www.pnas.org/content/110/14/5347.abstract>
- 471 Wang, B., Li, J., Cane, M. A., Liu, J., Webster, P. J., Xiang, B., et al. (2018). Toward Predicting
 472 Changes in the Land Monsoon Rainfall a Decade in Advance. *Journal of Climate*, 31(7), 2699–
 473 2714. JOUR. <https://doi.org/10.1175/JCLI-D-17-0521.1>
- 474 Wang, P. X., Wang, B., Cheng, H., Fasullo, J., Guo, Z., Kiefer, T., & Liu, Z. (2017). The global
 475 monsoon across time scales: Mechanisms and outstanding issues. *Earth-Science Reviews*, 174,
 476 84–121. JOUR. <https://doi.org/https://doi.org/10.1016/j.earscirev.2017.07.006>
- 477 Wang, Y., Li, S., & Luo, D. (2009). Seasonal response of Asian monsoonal climate to the Atlantic
 478 Multidecadal Oscillation. *Journal of Geophysical Research: Atmospheres*, 114(D2). JOUR.
 479 <https://doi.org/10.1029/2008JD010929>
- 480 Yeager, S., Karspeck, A., Danabasoglu, G., Tribbia, J., Teng, H., Yeager, S., et al. (2012). A Decadal
 481 Prediction Case Study: Late Twentieth-Century North Atlantic Ocean Heat Content. *Journal of*
 482 *Climate*, 25(15), 5173–5189. <https://doi.org/10.1175/JCLI-D-11-00595.1>
- 483 Yun, K.-S., & Timmermann, A. (2018). Decadal Monsoon-ENSO Relationships Reexamined.
 484 *Geophysical Research Letters*, 45(4), 2014–2021. JOUR. <https://doi.org/10.1002/2017GL076912>
- 485 Zhang, R., & Delworth, T. L. (2006). Impact of Atlantic multidecadal oscillations on India/Sahel
 486 rainfall and Atlantic hurricanes. *Geophysical Research Letters*, 33(17). JOUR.
 487 <https://doi.org/10.1029/2006GL026267>
- 488 Zhang, Y., Wallace, J. M., & Battisti, D. S. (1997). ENSO-like Interdecadal Variability: 1900–93.
 489 *Journal of Climate*, 10(5), 1004–1020. JOUR. [https://doi.org/10.1175/1520-](https://doi.org/10.1175/1520-0442(1997)010<1004:ELIV>2.0.CO;2)
 490 0442(1997)010<1004:ELIV>2.0.CO;2
- 491 Zhou, T., Zhang, L., & Li, H. (2008). Changes in global land monsoon area and total rainfall
 492 accumulation over the last half century. *Geophysical Research Letters*, 35(16). JOUR.
 493 <https://doi.org/doi:10.1029/2008GL034881>

494

495

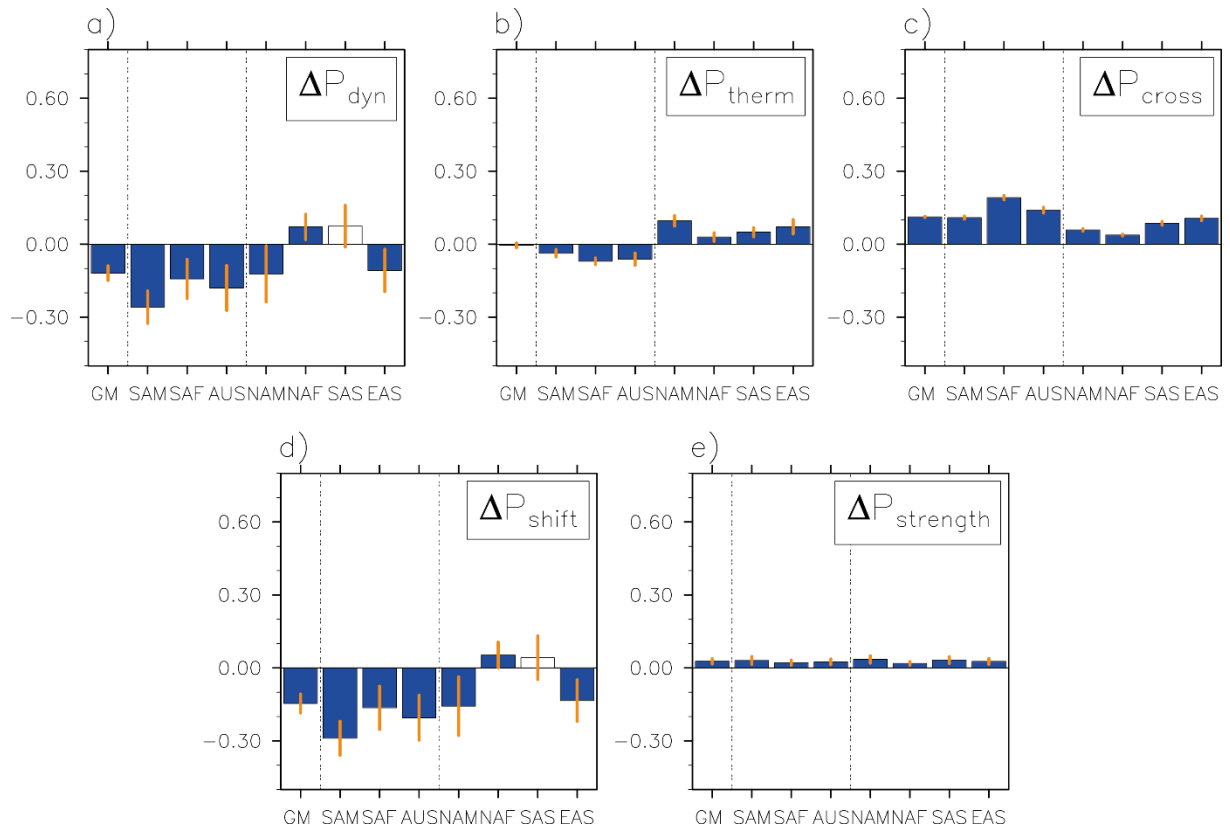


496

497 **Figure 1:** (a) Observed precipitation (mm.day⁻¹; GPCC; (Schneider et al., 2014)) regressed onto the
 498 AMV index (ERSST;(Huang et al., 2015)) (See the method in the supplementary material). (b) Change
 499 in precipitation (mm.day⁻¹) related to AMV (AMV+ minus AMV-). Monsoon domains are drawn in red

500 (see section 2.2 for details). Precipitation anomalies are shown for MJJAS (NDJFM) for the Northern
501 (Southern) Hemisphere. Stippling indicates that anomalies are significantly different to zero according
502 to a Student's t-test at the 95% confidence level. (c) Changes in monsoon index (MI; $\text{mm}\cdot\text{day}^{-1}$) for
503 AMV+ minus AMV-. A blue bar indicates significant changes according to a Student's t-test at the 95%
504 confidence level. Orange vertical lines show two standard errors. (d) Change in monsoon area (MA; %
505 of the Earth total surface) versus the change in monsoon precipitation (MP; total area weighed
506 precipitation, in $10^9 \text{ m}^3\cdot\text{day}^{-1}$). Vertical and horizontal colored lines indicate two standard errors for both
507 MP and MA. The black line is the MA—MP linear regression (excluding GM). For (c) monsoon
508 domains are not fixed and computed separately from each member and experiment.

509



510

511 **Figure 2:** Decomposition of precipitation anomalies ($\text{mm}\cdot\text{day}^{-1}$) into those due to (a) dynamic
 512 (ΔP_{dyn}) (b) thermodynamic (ΔP_{therm}) and (c) cross-term (ΔP_{cross}) terms, as defined in Chadwick et al.
 513 (2016). The dynamic part is decomposed into its (e) shift (ΔP_{shift} , i.e. due to a change in the pattern of
 514 the circulation) and (f) weak ($\Delta P_{\text{strength}}$, i.e. related to the strength of the mean tropical circulation)
 515 components. Orange vertical lines represent two standard errors. A blue bar is added when anomalies
 516 are stronger than two standard errors.

517

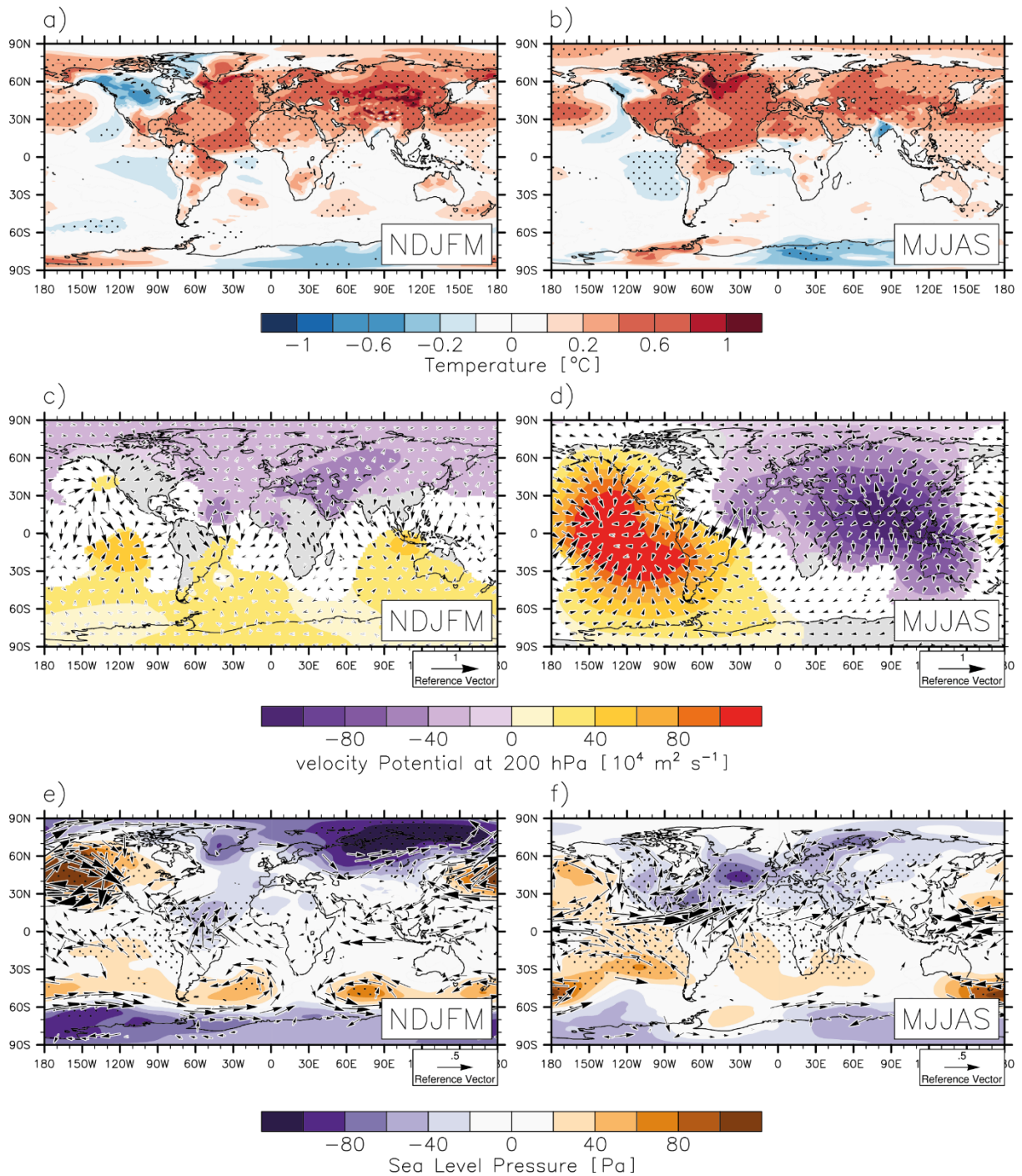
518

519

520

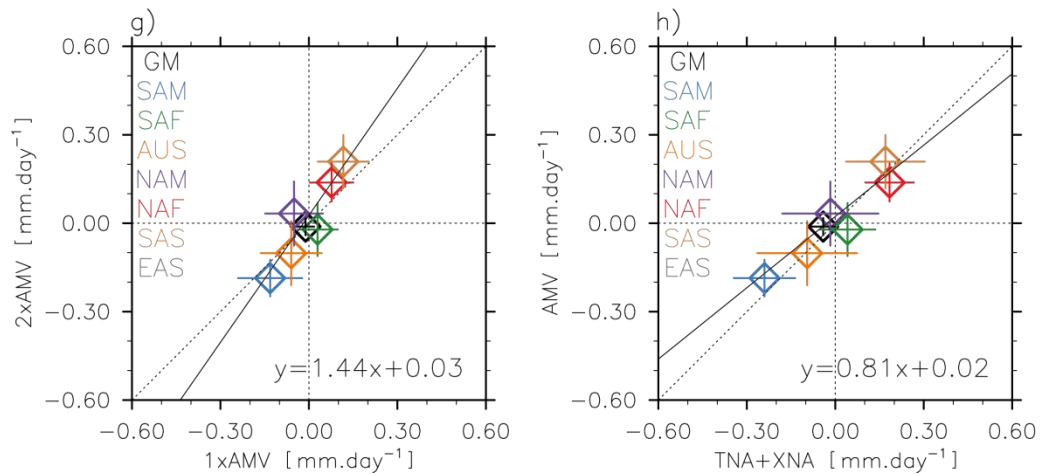
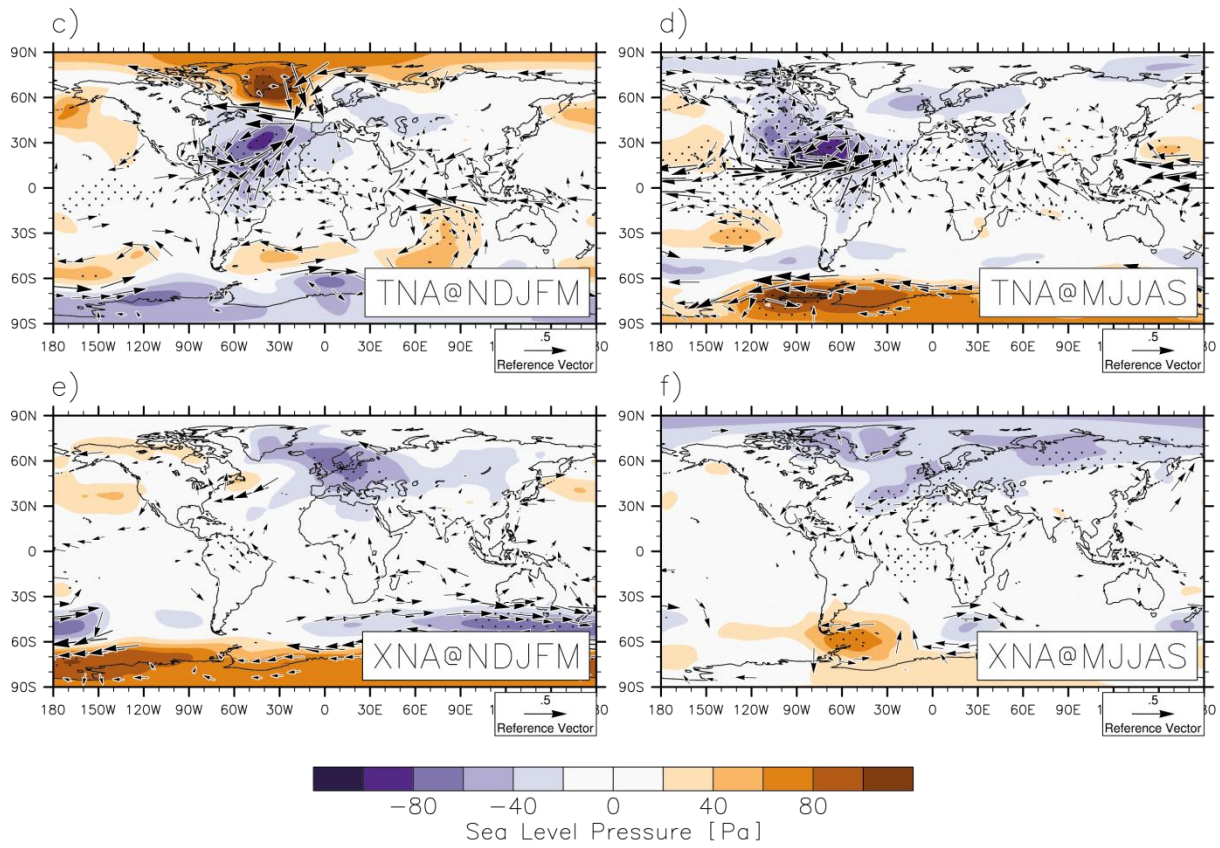
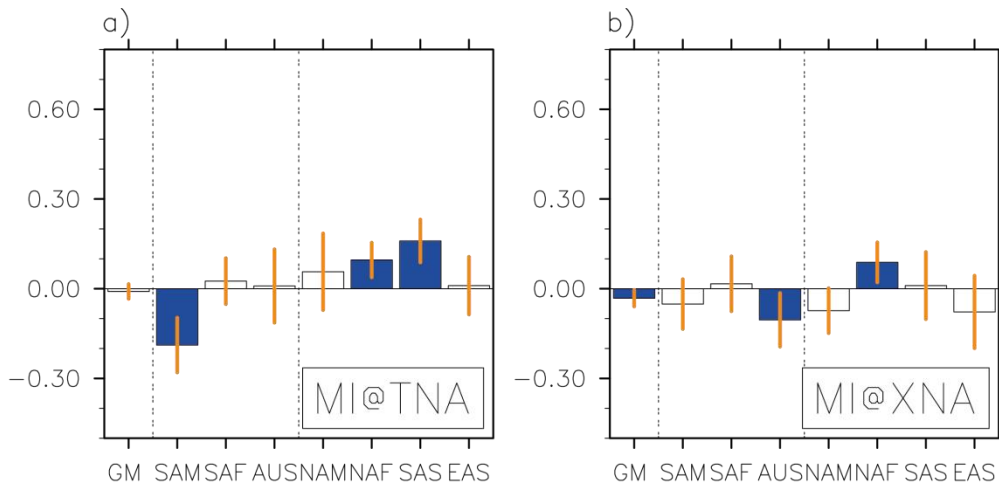
521

522



523

524 **Figure 3:** Effect of AMV on (top panels) surface temperature ($^{\circ}\text{C}$), (middle) 250 hPa velocity potential
 525 (in $10^4 \text{ m}^2 \text{ s}^{-1}$) and divergent wind ($\text{m} \cdot \text{s}^{-1}$) and (bottom) sea level pressure (Pa) and 850 hPa wind ($\text{m} \cdot \text{s}^{-1}$), in (left) NDJFM and (right) MJJAS. Stippling (shading) for surface temperature (velocity potential)
 526 indicates that changes are significantly different to zero according to a Student's t-test at the 95%
 527 confidence level. For the 850 hPa wind, arrows are drawn only if their meridional or zonal components
 528 are significantly different to zero, according to a Student's t-test at the 95% confidence level.
 529



531 Figure 4: Top panels: same as in figure 1b but for (a) the tropical Atlantic Ocean warming (TNA+ minus
532 TNA-) and (b) due to the extratropical Atlantic Ocean warming (XNA+ minus XNA-). Middle panels:
533 same as in figure 3a and figure 3b, but for TNA and XNA. Bottom panels: effect of 2xAMV on MI in
534 function of the effect of (left) 1xAMV on MI (right) the TNA+XNA sum on MI. Vertical and horizontal
535 black lines indicate the spread in MI, and the black line is the linear regression, as computed from the
536 sub-domain monsoons only (e.g. excluding GM). Significance in panels a-f are calculated using a
537 Student's t-test at the 95% confidence level.